ChemComm

FEATURE ARTICLE

View Article Online
View Journal | View Issue

Check for updates

Cite this: *Chem. Commun.*, 2025, **61**, 3271

Catalytic reduction of $NAD(P)^+$ to NAD(P)H

Shunichi Fukuzumi, *[ab] Yong-Min Lee *[ac] and Wonwoo Nam *[a]

Received 25th November 2024,
Accepted 14th January 2025

DOI: 10.1039/d4cc06254j

rsc.li/chemcomm

1,4-Dihydronicotinamide adenine dinucleotide (NADH) and its phosphate ester (NADPH) are essential cofactors required for all living cells, playing pivotal roles in multiple biological processes such as energy metabolism and biosynthesis. NADPH is produced during photosynthesis by the combination of photosystem II, where water is oxidised, and photosystem I, where $NADP^+$ is reduced. This review focuses on catalytic $NAD(P)^+$ (and its analogues) reduction to generate 1,4-NAD(P)H without formation of other regioisomers and the dimer. There are different ways for production of 1,4-NAD(P)H and its analogues. Firstly, electrocatalytic reduction of $NAD(P)^+$ is discussed to clarify how the regioselective reduction of $NAD(P)^+$ to 1,4-NAD(P)H is achieved with use of metal complex catalysts. The applied potential for the electrocatalytic reduction of $NAD(P)^+$ to 1,4-NAD(P)H is much reduced by combination with the photocathode under photoirradiation. Then, mechanisms of hydrogenation of $NAD(P)^+$ by H_2 and transfer hydrogenation of $NAD(P)^+$ by formate used as an electron and proton source to produce 1,4-NAD(P)H are discussed. Hydroquinone derivatives are also used as plastoquinol analogues, which act as hydride sources in a photosystem I model reaction, in which $NAD(P)^+$ and its analogues are reduced by hydroquinone derivatives to form 1,4-NAD(P)H and its analogues using an $NAD(P)^+$ reduction catalyst and a photoredox catalyst. The photosystem I model is then combined with a photosystem II model in which plastoquinone analogues are reduced to plastoquinol analogues by water to achieve the stoichiometry of photosynthesis, that is, photocatalytic reduction of $NAD(P)^+$ by water.

[a] *Department of Chemistry and Nanoscience, Ewha Womans University, Seoul 03760, Korea. E-mail: fukuzumi@chem.eng.osaka-u.ac.jp, yomlee@ewha.ac.kr, wwnam@ewha.ac.kr*
[b] *Department of Chemistry, University of Tsukuba, Tennodai, Tsukuba, Ibaraki 305-8571, Japan*
[c] *Research Institute for Basic Sciences, Ewha Womans University, Seoul 03760, Korea*

1. Introduction

Cytochrome *c* oxidase requires 1,4-dihydonicotinamide adenine dinucleotide (NADH; see Fig. 1) as an e^- and H^+ source for the catalytic $4e^-/4H^+$ reduction of dioxygen to water.[1–6] Cytochrome P-450 enzyme also requires NADPH (Fig. 1) to

Shunichi Fukuzumi

Shunichi Fukuzumi received his BS degree in 1973 and PhD degree in 1978 from the Tokyo Institute of Technology. After working as a postdoctoral fellow (1978–1981) at Indiana University in the United States, he joined Osaka University as an assistant professor in the Department of Applied Chemistry in 1981. He was promoted to a Full Professor at Osaka University in 1994. His research interests are electron-transfer chemistry, redox catalysis, and artificial photosynthesis. He is a Distinguished Professor of Ewha Womans University and Professor Emeritus of Osaka University.

Yong-Min Lee

Yong-Min Lee received his PhD degree from Pusan National University, Korea (Major: Inorganic Chemistry), under the supervision of Professor Sung-Nak Choi in 1999. Then, he joined the Centro di Ricerca di Risonanze Magnetiche (CERM) at Università degli Studi di Firenze, Italy, as a postdoctoral fellow and researcher under the supervision of Professors Claudio Luchinat and Ivano Bertini (from 1999 to 2005). In 2006, he moved to Center for Biomimetic Systems at Ewha Womans University, as a Research Professor. Since 2009, he has been a Professor for Special Appointment at Ewha Womans University.

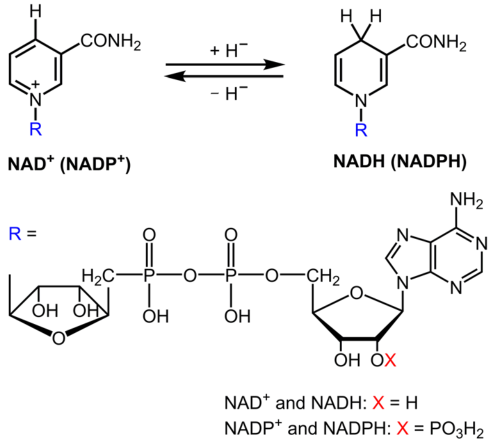

Fig. 1 Structural forms of $NAD(P)^+$ and NAD(P)H.

reductively activate dioxygen for the catalytic oxygenation reactions.[7–12] NADPH is produced by the regioselective $NADP^+$ reduction by plastoquinol in photosystem I (PSI) *via* a ferredoxin-NADPH reductase (FNR), which ultimately reduces $NADP^+$ into NADPH, whereas plastoquinol is formed by the photocatalytic reduction of plastoquinone by water in photosystem II (PSII) during photosynthesis.[13–16] Overall NADPH is produced by the regioselective reduction of $NADP^+$ using water as an e^- and H^+ source in photosynthesis [eqn (1)].[13–16] Many industrially relevant enzymes depend on the cofactors NADH and NADPH, which are too expensive to be added in stoichiometric amounts.[17–23] Therefore, extensive efforts have been made to develop efficient catalytic systems for NAD(P)H recycling with high activity without producing by-products such as the NAD(P) dimer and other regioisomers (1,2- and 1,6-dihydro forms).[24–30]

This Feature Article has focused on catalytic production of 1,4-NAD(P)H by electrocatalytic reduction of $NAD(P)^+$, hydrogenation of $NAD(P)^+$ and photocatalytic reduction of $NAD(P)^+$ to 1,4-NAD(P)H by electron donors including plastoquinol analogues with use of photoredox catalysts to mimic the molecular function of PSI.[31] The catalytic mechanism is discussed to clarify how the regioselective $NAD(P)^+$ reduction to the 1,4-dihydro form, NAD(P)H, is possible by the catalysts. Finally a PSII model, in which H_2O is oxidized by a plastoquinone (PQ) analogue to produce O_2 and a plastoquinol (PQH_2) analogue,[32,33] has been combined with the PSI model to achieve the stoichiometry of the photosynthesis, *i.e.*, the photocatalytic reduction of $NAD(P)^+$ by H_2O to produce O_2 and NAD(P)H [eqn (1)].[31] Once NAD(P)H is produced by using H_2O, combination of NAD(P)H dependent enzymes would make it possible to use H_2O as a reductant for recycling NAD(P)H in a large number of industrial enzymatic reactions.

$$2H_2O + 2NAD(P)^+ \xrightarrow{h\nu} O_2 + 2NAD(P)H + 2H^+ \qquad (1)$$

Wonwoo Nam

Wonwoo Nam earned his BS (Honors) degree in Chemistry from California State University, Los Angeles (1985), and his PhD degree in Inorganic Chemistry from UCLA (1990). After postdoctoral experience at UCLA, he became an Assistant Professor at Hong Ik University in 1991. He moved to Ewha Womans University in 1994, where he is presently a Distinguished Professor. His current research focuses on the mechanism of dioxygen activation and water oxidation in biomimetic and bioinorganic chemistry.

2. Electrocatalytic reduction of $NAD(P)^+$

One method for nonenzymatic production of NAD(P)H is electrocatalytic reduction of $NAD(P)^+$, although the production of NAD(P)H isomers remains a difficult issue.[34–37] Electrocatalytic reduction of NAD^+ to 1,4-NADH was reported with use of Cu, Fe, Co, and carbon electrodes.[38] Fig. 2 shows the reduction of NAD^+ to different NADH isomers and the dimer when NAD^+ is totally consumed after the electrocatalytic reduction at different applied potentials.[38] The highest yield of 1,4-NADH using Cu, Fe, and Co electrodes was obtained as 58%, 64% and 49% at −0.4 V *vs.* RHE, respectively. In contrast to regioselective reduction of NAD^+ at the metal electrodes, the yield of 1,4-NADH was much smaller (7.9%) at −0.4 V (*vs.* RHE) at the

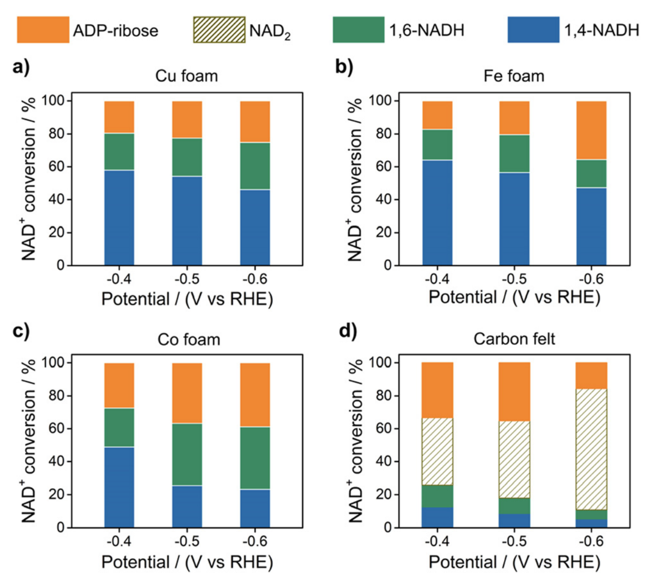

Fig. 2 Product yields obtained in the electrocatalytic reduction of NAD^+ using (a) Cu, (b) Fe, (c) Co and (d) carbon electrodes depending on the applied potentials (pH 7; [phosphate buffer] = 0.10 M and $[NAD^+]_{ini}$ = 1.0 mM). Reprinted with permission from ref. 38. Copyright 2022, Royal Society of Chemistry.

carbon electrode, which has a high proportion of the dimeric product (NAD_2 > 40%). ADP-ribose was also produced probably by the fragmentation of NAD^+.[38]

Because no NAD_2 was produced in the electrocatalytic reduction of NAD^+ with use of Cu, Fe, and Co electrodes (Fig. 2), it has been proposed that the surface-adsorbed hydrogen atom [$*H_{ad}$: asterisk (*) denotes the active site] is produced on Cu, Fe, and Co electrodes *via* proton-coupled electron transfer (step 1), followed by the reaction of $*H_{ad}$ with NAD^+ coupled with electron transfer (step 2) as shown in Scheme 1.[38] The poor proton activation ability of the carbon electrode results in a low coverage of H_{ad}, when the electron-transfer reduction of NAD^+ proceeds to produce NAD_2 (step 2b in Scheme 1).[38–41] The low selectivity to 1,4-NADH production in Fig. 2 should be improved for any application.

A cathode made from MWCNTs containing Ni nanoparticles (NP), Ni NP-MWCNTs (Scheme 2), was employed for the electrocatalytic reduction of NAD^+ to produce 98% 1,4-NADH at a potential that is 700 mV more positive than that on carbon nanofibres (CNFs) and pure MWCNTs.[42] The highly efficient production of 1,4-NADH on Ni NP-MWCNTs at low cathodic overpotentials results from the adsorption of activated hydrogen (H_{ads}) on the NP-MWCNT electrode at low overpotentials, which facilitates the hydrogenation of NAD^+ to produce 1,4-NADH.[42]

The incorporation of Ni nanoparticles (NPs) on TiO_2 (Ni-TOTs) was reported to enhance the selective hydrogenation of NAD^+ stabilized on TiO_2 to produce high yield of the enzymatically active 1,4-NADH (93.8% at −0.9 V *vs.* Ag/AgCl).[43] The Ti^{3+} and oxygen vacancies are suggested to play a crucial role in NAD^+ adsorption, facilitating the selective hydrogenation by Ni-TOTs.[43]

The regioselective electrocatalytic reduction of NAD^+ to 1,4-NADH was achieved with use of $[Rh(bpy)_2]^+$ (bpy = 2,2′-bipyridine),

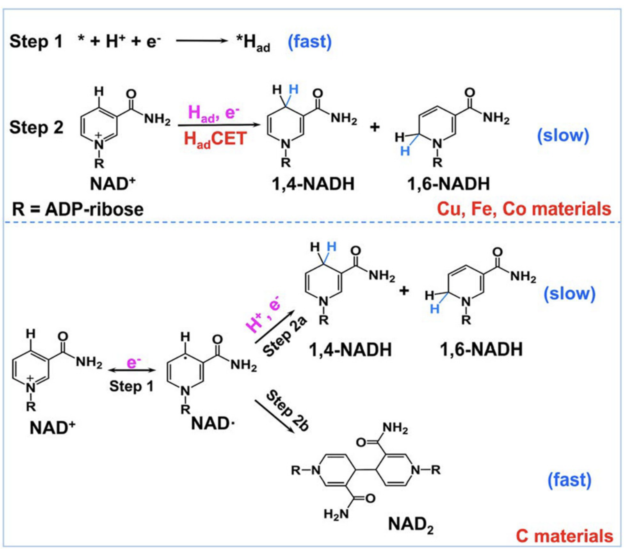

Scheme 1 Proposed NAD^+ reduction mechanism at H_{ad}-rich Cu, Fe, and Co electrodes (top) and H_{ad}-poor C material electrodes (bottom). Reprinted with permission from ref. 38. Copyright 2022, Royal Society of Chemistry.

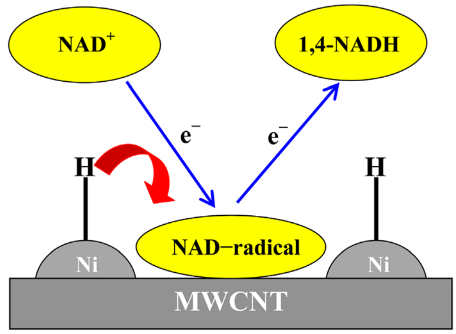

Scheme 2 The Ni NP-MWCNT electrode used for electrocatalytic production of 1,4-NADH. Reprinted with permission from ref. 42. Copyright 2017, John Wiley and Sons.

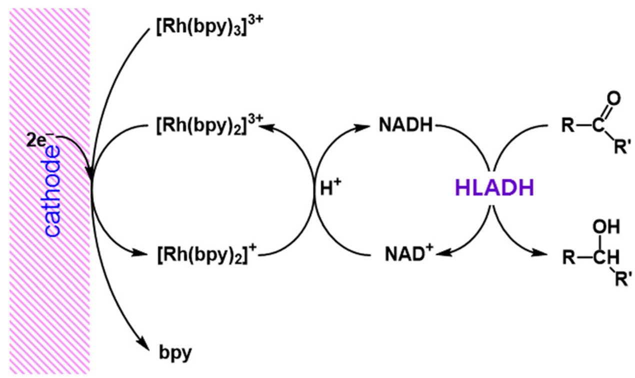

Scheme 3 Electrocatalytic production of NADH from NAD^+ using $[Rh(bpy)_2]^+$.[44]

which was produced by the electrochemical two-electron reduction of $[Rh(bpy)_3]^{3+}$, accompanied by release of a bpy ligand.[44] The produced NADH is oxidised by cyclohexanone under catalysis of horse liver alcohol-dehydrogenase (HLADH) (Scheme 3).[44]

The aquo-(2,2′-bipyridine)(pentamethylcyclopentadienyl)-rhodium(III) complex ($[Cp^*Rh(bpy)(H_2O)]^{2+}$) was also reported to act as an extremely effective redox catalyst for the electrocatalytic production of 1,4-NADH as well as for the chemical reduction of $NAD(P)^+$ with formate as a hydride donor.[45,46] The catalytic mechanism of the regioselective reduction of NAD^+ with $[Cp^*Rh(bpy)(H_2O)]^{2+}$ was proposed as shown in Scheme 4, where a Rh(III)-hydride complex ($[Cp^*Rh(bpy)H]^+$) was produced by the reaction of formate with $[Cp^*Rh(bpy)(H_2O)]^{2+}$. $[Cp^*Rh(bpy)H]^+$ was converted to a Rh(I) complex with an η^4-pentamethylcyclopentadiene ligand having a new C–H bond *endo* with respect to the metal centre ($[(Cp^*H)Rh^I(bpy)]^+$).[28,47,48] The X-ray crystal structure of $[(Cp^*H)Rh^I(bpy)]^+$ is shown in Fig. 3a, where the C1–C2 distance (1.517(2) Å) is longer than the C2–C3 (1.440(3) Å) distance, confirming the diene structure.[48] In sharp contrast, the crystal structure of the Cp*Rh(I) complex (Fig. 3b) shows only a 0.034 Å difference in the cyclopentadienyl C–C bonds.[49] The coordination of the amide group of NAD^+ to the Rh centre of $[(Cp^*H)Rh(bpy)]^+$ results in the regioselective reduction of NAD^+ to 1,4-NADH, followed by the replacement

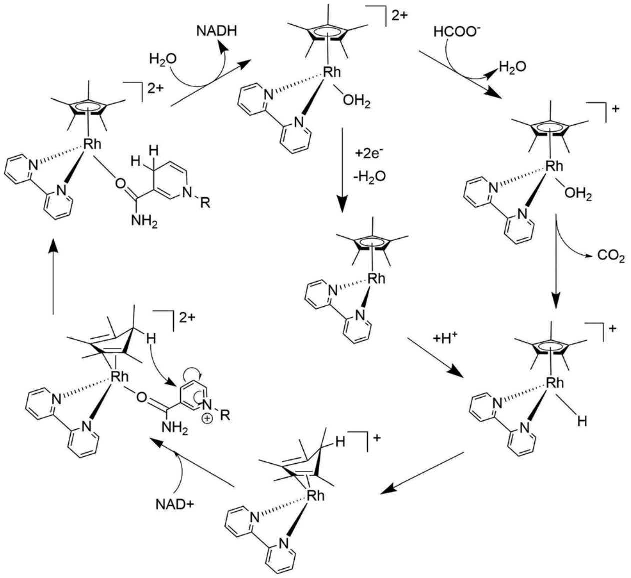

Scheme 4 Proposed mechanism of catalytic hydrogenation of NAD^+ by formate to 1,4-NADH with $[Cp^*Rh(bpy)(H_2O)]^{2+}$. Reprinted with permission from ref. 48. Copyright 2016, Royal Society of Chemistry.

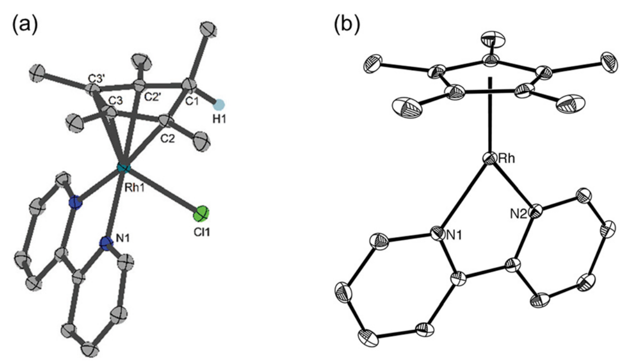

Fig. 3 X-ray structures of (a) $[(Cp^*H)Rh(bpy)]^+$ and (b) $[Cp^*Rh(bpy)]^+$. Reprinted with permission from ref. 48. Copyright 2016, Royal Society of Chemistry.

of 1,4-NADH by H_2O to regenerate $[Cp^*Rh^{III}(bpy)(H_2O)]^{2+}$ (Scheme 4).[47,48]

The immobilization of a rhodium complex with a pyrene-substituted phenanthroline ligand (pyr-Rh) was performed on multi-walled carbon nanotubes (MWCNTs) *via* π–π stacking to enhance the stability of the catalyst for the electrocatalytic production of NADH (Scheme 5).[50] The pyr-Rh/MWCNT electrodes can also be applied to produce 1,4-NADH for enzymatic synthesis in which malate dehydrogenase (MDH) was incorporated for enzymatic reduction of oxaloacetic acid.[50]

The $[Rh(Cp^*)(bpy)Cl]^+$ complex was also immobilised on highly ordered three dimensional (3D) metal–organic framework (NU-1000) films at the zirconium nodes of NU-1000 (*vide infra*).[51] The glassy carbon (GC) electrode was modified with carboxyl groups by electrochemical oxidation of 4-aminobenzoic acid (GC-COOH).[51] An NU-1000 film was produced through the coordination by a Zr-oxo cluster (GC-Zr), followed by solvothermal

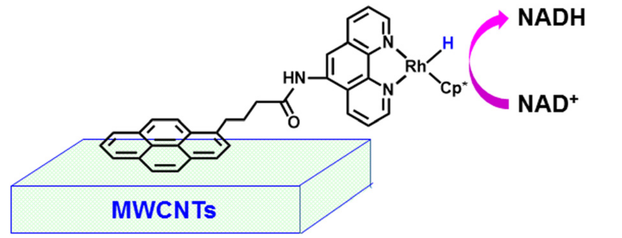

Scheme 5 Immobilization of the pyr-Rh complex onto MWCNTs.

synthesis (GC-NU1000).[51] The NU-1000 film provided a 3D framework with regularly positioned nodes, where catalysts are loaded.[51] The carboxyl-functionalized-Rh catalyst (Rh-COOH) was anchored onto the nodes of the film by solvent-assisted ligand incorporation (SALI) to prepare the Rh-immobilized electrode (GC-NU1000-Rh in Scheme 6).[51] Electrocatalytic NAD^+ reduction to 1,4-NADH was performed using GC-NU1000-Rh at an applied potential of −0.72 V in 30 mL of Tris buffer (pH 7.2) to afford a high TOF (∼1400 h^{-1}) as well as a high faradaic efficiency (97%).[51] This was coupled with an electroenzymatic conversion of pyruvate into L-lactate with a total TON of over 20 000 using L-lactate dehydrogenase.[51]

Prominent synergetic effects between various metal electrodes (Cu, Fe, Co, and Ni) and $[Cp^*Rh(bpy)(H_2O)]Cl_2$ (or $[Cp^*Rh(phen)(H_2O)]Cl_2$) in electrolytes were reported for electrocatalytic reduction of NAD^+ to 1,4-NADH.[52] For example, the normalized activity of the Cu-$[Cp^*Rh(bpy)(H_2O)]Cl_2$ (Cu-M) system was 16 times higher than that of $[Cp^*Rh(bpy)(H_2O)]Cl_2$ alone, whereas Cu alone showed trace catalytic activity at the same applied potential.[52] The maximal selectivity of 1,4-NADH was enhanced from 63% for Cu alone to 95.3% for the coupled system.[52] The Rh-hydride complex may be formed *via* adsorbed hydrogen (H_{ad}) on Cu and electron transfer, catalysing the NAD^+ reduction to 1,4-NADH, whereas there is negligible H_{ad} on the surface of the carbon electrode (Scheme 7).[52]

Ni sulfides (Ni_3S_2 and NiS_2) were efficient for direct NAD^+ reduction, but the selectivity to produce 1,4-NADH was not high.[53] The coupled system of the Ni_3S_2 electrode and $[Cp^*Rh(bpy)(H_2O)]Cl_2$ has enabled the NAD^+ reduction to 1,4-NADH with both the highest activity and selectivity among previously reported results.[53] In the direct NAD^+ reduction on Ni_3S_2 in the absence of the Rh complex, the reaction proceeds

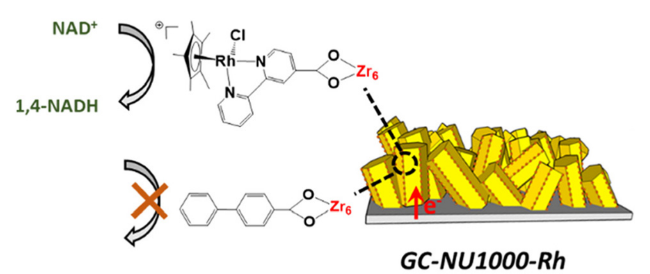

Scheme 6 Electrocatalytic reduction of NAD^+ to 1,4-NADH with use of a $[Rh(Cp^*)(bpy)Cl]^+$-functionalised NU-1000 film on a GC electrode (GC-NU1000-Rh). Reprinted with permission from ref. 51. Copyright 2022, American Chemical Society.

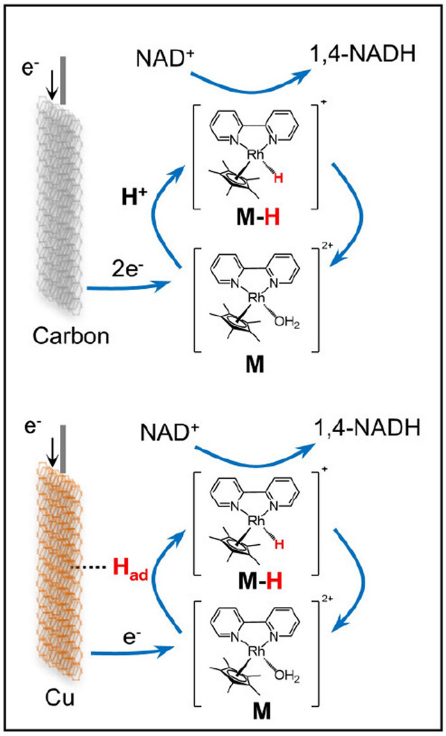

Scheme 7 Schematic description of the electrocatalytic NADH regeneration reaction with [Cp*Rh(bpy)(H_2O)]Cl_2 (M) alone and the Cu-M system. Reprinted with permission from ref. 52. Copyright 2024, American Chemical Society.

via a hydride-transfer process or an H_{ad}-coupled electron transfer mechanism, suppressing the formation of $NAD^{\bullet}$ and thereby preventing the production of byproduct NAD_2 (Scheme 8a).[53] However, the selectivity in 1,4-NADH is only 80% for Ni_3S_2.[53] The low selectivity to produce 1,4-NADH is a common issue in the direct electrocatalytic reduction of NAD^+ with heterogeneous catalysts.[38–42,52–56] In the carbon-Rh electrode system, the NAD^+ reduction proceeds *via* a hydride transfer from the Rh–hydride complex, but the carbon electrode is only a conductive electrode providing electrons to the Rh complex.[54] A hydride transfer mechanism has been well established for the Rh-, Ru- and Ir-catalysed chemical reduction of NAD^+ with formate as a reductant.[57–68] In the Ni_3S_2-Rh system, Ni_3S_2 can transfer electrons and active hydrogen atoms to Rh efficiently *via* a concerted electron–proton transfer (CEPT) mechanism (Scheme 8b).[53]

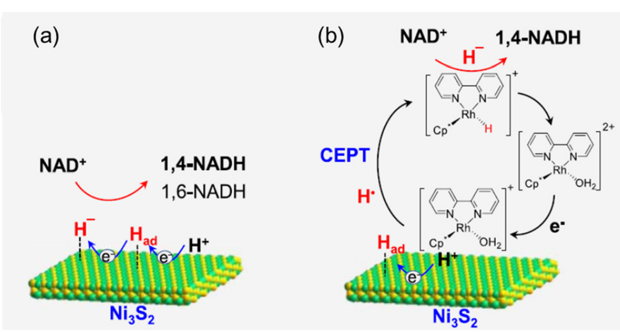

Scheme 8 Proposed mechanisms of NAD^+ reduction into NADH for (a) Ni_3S_2 alone and (b) the Ni_3S_2-Rh system. Reprinted with permission from ref. 53. Copyright 2024, American Chemical Society.

3. Photoelectrocatalytic reduction of NAD(P)$^+$

The photovoltage (V_{ph}) of the p-type silicon nanowire (p-SiNW) photocathode composed of a buried n^+p radial junction was enhanced for NADH production under solar light irradiation as shown in Scheme 9, where introduction of an n^+ layer into p-SiNW results in an increase in the band bending at the n^+/p interface to enhance the p-SiNW's V_{ph} (435 mV).[69] Electron transfer from the photoexcited electrons to $[Cp^*Rh(bpy)(H_2O)]^{2+}$ (M_{ox} mediator) afforded a benchmark onset potential (E_{onset}) of 0.393 V compared to the reversible hydrogen electrode (RHE) among reported SiNW-based photocathodes.[69–72] Thus, the n^+p-SiNW photocathode achieved M_{red}-mediated regioselective conversion of NAD^+ to 1,4-NADH to afford a faradaic efficiency (FE) of 85% and a conversion rate of 1.6 μmol h^{-1} cm^{-1} at 0.2 V *vs.* RHE. The photoelectrocatalytic activity for NADH production remained for at least 12 h at the low cathodic potential.[69]

In PSI, photoinduced electron transfer from P700 in the thylakoid membrane to ferredoxin (Fd) occurs, followed by subsequent electron transfer to ferredoxin-$NADP^+$ reductase (FNR), catalysing the solar-driven reduction of $NADP^+$ to 1,4-NADPH (Fig. 4a).[73,74] Inspired by the efficient photocatalytic function of PSI, an alkane-chain-substituted Rh1 complex ([Rh(Cp*)-(bpy)Cl]$^+$) was self-assembled on aliphatic chain-modified micro-pyramid p-type silicon array (p-Si) photocathodes (Fig. 4b).[73] An electron-transfer mediator 4,4′-(1,4-phenylene)bis(1-octyl-pyridin-1-ium) (OBV^{2+}) was employed to facilitate electron transfer from OBV^{2+} to the catalytic components. Rh1 and OBV^{2+} were assembled on the surface of SCA-modified p-Si *via* hydrophobic interactions to obtain electrode-supported "lipid-bilayer membrane" photocathodes.[73] The incident photon-to-current efficiency (IPCE) of Rh1/OBV^{2+}/SCA/p-Si for the photoelectrocatalytic

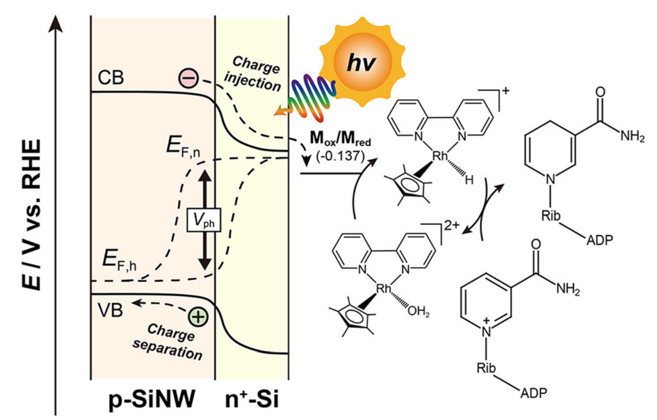

Scheme 9 Reaction scheme of photocatalytic production of NADH at the photocathode driven by n^+p-SiNWs. Reprinted with permission from ref. 69. Copyright 2023, American Chemical Society.

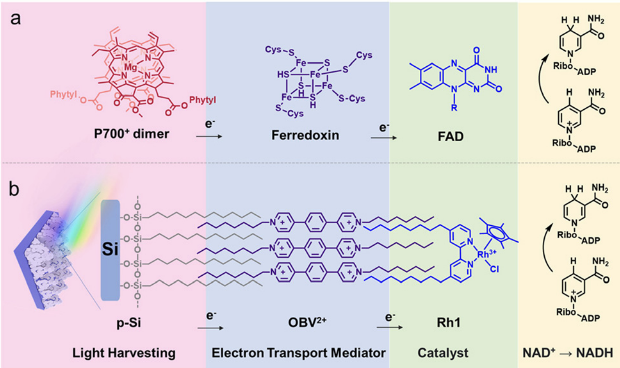

Fig. 4 (a) Electron flow from the PSI component to Fd and FAD. (b) Schematic of the photocathode with a lipid-bilayer membrane. Reprinted with permission from ref. 73. Copyright 2024, Royal Society of Chemistry.

reduction of NAD^+ to 1,4-NADH was always higher than that of Rh1/SCA/p-Si over the entire spectral range.[73] The IPCE of Rh1/OBV^{2+}/SCA/p-Si at 665 nm was determined to be 3.2%, which was significantly larger than the IPCE of Rh1/SCA/p-Si (1.55%), because of the promotion of the photoinduced electron transfer and inhibition of interfacial charge recombination between the p-Si semiconductor and Rh1 catalyst.[73] Thus, OBV^{2+} plays an important role as an electron mediator as compared with the photoelectrode without an electron mediator (Scheme 9).[69,73]

4. Catalytic hydrogenation of NAD(P)$^+$

Hydrogenation of NAD^+ by H_2 with $[M_2\text{-}OH_2]^0$ occurred under basic conditions (*e.g.*, pH = 8) to produce 1,4-NADH regioselectively.[75] The yield of 1,4-NADH based on the initial mol% amount of NAD^+ and the turnover number (TON) reached 97% and 9.3 (90 min), respectively.[75] The turnover frequency (TOF) of H_2 evolution from NADH increased with decreasing pH in the region between 4.1 and 7.0, which overlaps with the ratio of $[M_1\text{-}OH_2]^+$, whereas the pH dependence of TOF for hydrogenation of NAD^+ overlaps with the ratio of $[M_2\text{-}OH_2]^0$.[75] At pH 6.5, the TOF for the NADH formation was determined to be 36 h^{-1}, whereas the TOF for the H_2 evolution reached 52 h^{-1} at pH 4.1.[75] Such pH dependence of TOF indicates that $[M_1\text{-}OH_2]^+$ reacts with NADH to produce H_2 and that $[M_2\text{-}OH_2]^0$ reacts with H_2 to reduce NAD^+ to NADH, similar to the case of interconversion between HCOOH and H_2 with use of the same Ir catalyst.[76]

The rate-determining step in the catalytic hydrogenation of NAD^+ with hydrogen is the reaction of the Ir–H_2O complex with H_2 to form the Ir(III)-hydride complex, followed by fast hydride transfer to NAD^+ to produce 1,4-NADH (the right-hand catalytic cycle in Scheme 10).[75] Formation of the Ir(III)-hydride complex under normal pressure of hydrogen was detected by ^{1}H-NMR, ESI mass, and UV-vis spectroscopies.[75] This is the first demonstration of the interconversion between NADH and H_2 using a water-soluble iridium-aqua complex, in which H_2 is oxidized by NAD^+ to produce H^+ and NADH, whereas H_2 and NAD^+ are

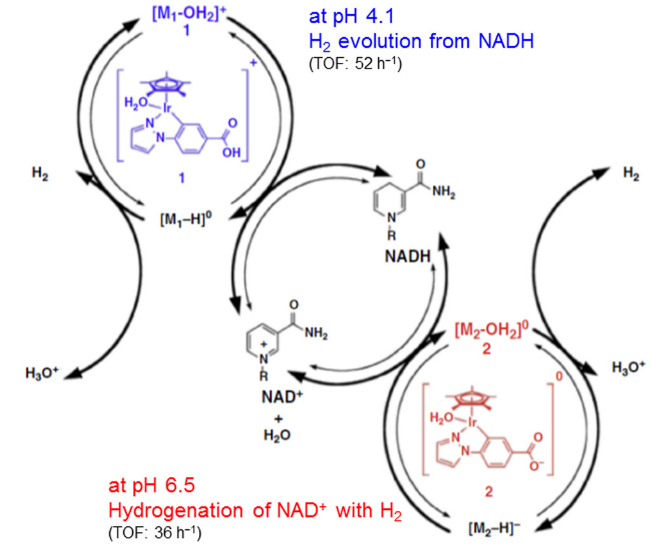

Scheme 10 Proposed mechanism for catalytic interconversion between NADH and H_2 with use of water soluble [C,N] cyclometalated Ir complexes (**1** and **2**) depending on pH. Reproduced with permission from ref. 75. Copyright 2011, American Chemical Society.

produced *via* the reduction of H^+ by NADH, depending on pH, under normal pressure at room temperature.[75]

Enzyme-metal biohybrids composed of NAD^+ reductase (NRase), biocatalytically synthesized small gold nanoparticles (Au NPs, <10 nm) and core–shell gold–platinum (Au@Pt) NPs were synthesized for tandem catalysis of hydrogenation of NAD^+ with H_2.[77] As shown in Scheme 11a, electrons released in the oxidation of NADH with NRase were used for the reduction of metal salts (M^{n+}) to produce biohybrid Au NPs, Au core, and (Au@Pt) NPs.[77] Au@Pt NPs prepared using NRase enzyme can re-donate electrons to NRase by utilizing its H_2 oxidation properties at 1 bar and 25 °C, thereby selectively reducing NAD^+ to the biologically active NADH cofactor (Scheme 11b).[77] At [NRase] = 1.9 mg mL^{-1}, 1,4-NADH was produced regioselectively, providing a novel route for continuous and H_2-driven efficient NADH recycling.[77] The H_2-driven

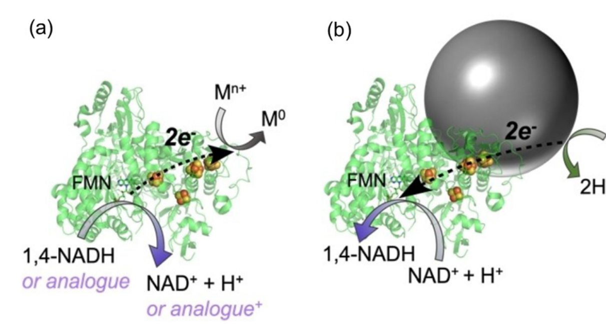

Scheme 11 (a) Formation of metal nanoparticles (MNPs) using NRase and NADH (or its analogue) as a reducing agent, while reducing M^{n+} to M^0. (b) Reduction of NAD^+ to NADH by H_2 *via* H_2 oxidation at the metal NP surface. Reprinted with permission from ref. 77. Copyright 2024, John Wiley and Sons.

1,4-NADH recycling was further coupled with alcohol dehydrogenase (YADH) for the reduction of enantioselective ketone.[77] Use of H_2 as a reductant for production of NADH has been previously explored using intact soluble hydrogenase enzymes[78] and co-immobilised hydrogenase and NRase on carbon particles.[79]

It has been reported that the simultaneous coupling of $[Cp^*Rh(bpy)(H_2O)]^{2+}$ and supported Ru NPs enhanced both catalytic activity and regioselectivity for the hydrogenation of $NAD(P)^+$, suggesting the efficient synergistic effect of the H_2 dissociation ability of supported Ru NPs and the steric effect of $[Cp^*Rh(bpy)(H_2O)]^{2+}$ in reducing $NAD(P)^+$ to 1,4-NAD(P)H.[80] NAD^+ could be completely converted to 1,4-NADH at 25 °C and 1 bar H_2 (>99% selectivity).[80] NADPH with >95% yield was also successfully reproduced by use of this coupling system.[80] The catalytic mechanism was proposed as shown in Fig. 5, where H_2 was first dissociated into adsorbed hydrogen (H*) over Ru NPs. $[Cp^*Rh(bpy)(H_2O)]^{2+}$ was reduced by H* to produce $[Cp^*Rh(\text{I})(bpy)]^0$, which was deposited on the surface of Ru NPs (Fig. 5).[80] $[Cp^*Rh(\text{I})(bpy)]^0$ reacted with protons to produce $[Cp^*Rh(bpy)H]^+$.[80] Then, hydride transfer from $[Cp^*Rh(bpy)H]^+$ to $NAD(P)^+$ occurred *via* a ring-slipped mechanism,[48] accompanied by regeneration of $[Cp^*Rh(bpy)(H_2O)]^{2+}$.[80] Nickel nanoparticles (NP) and $[Cp^*Rh(bpy)(H_2O)]^{2+}$ were also integrated for H_2-driven NAD(P)H regeneration through the immobilization of a Rh complex on a Ni/TiO_2 surface *via* a bipyridine containing 3D porous organic polymer (POP).[81]

Monocarbonyl diphosphine Ru(II) complexes were reported to be active for the regioselective reduction of NAD^+ to 1,4-NADH by formate as the hydride source in aqueous media.[82] The catalytic cycle is shown in Scheme 12, where the Ru(II) complexes react with formate to afford the hydride ruthenium complexes *via* β-hydride elimination accompanied by CO_2 evolution.[82] The hydride complexes hydrogenate NAD^+ to produce 1,4-NADH, accompanied by regeneration of the Ru(II) aqua complex (Scheme 12).[82] The Ru(II) aqua complex with the picolinamidate (pica) ligand was the most active, exhibiting a TOF of 6.08 h^{-1} in deuterated phosphate-buffered saline (PBS) at room temperature.[82]

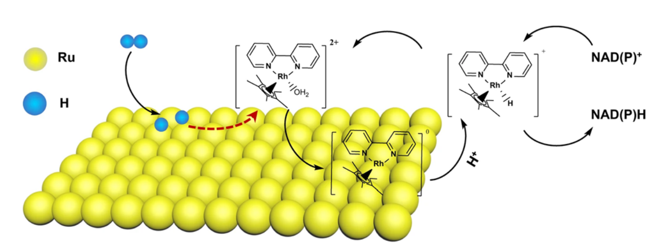

Fig. 5 Coupling of $[Cp^*Rh(bpy)(H_2O)]^{2+}$ and supported Ru NPs for $NAD(P)^+$ hydrogenation. Reprinted with permission from ref. 80. Copyright 2022, Springer Nature.

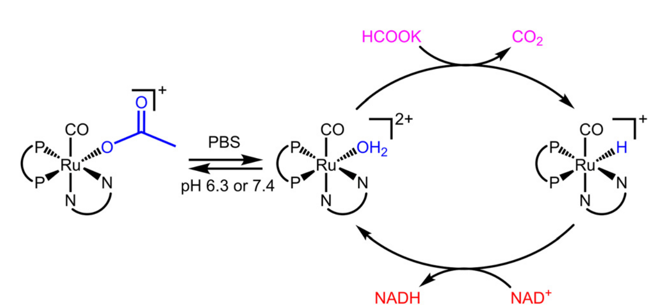

Scheme 12 Proposed catalytic pathway for the reduction of NAD^+ with monocarbonyl diphosphine Ru(II) complexes in PBS. Reproduced with permission from ref. 82. Copyright 2023, American Chemical Society.

5. Photocatalytic reduction of $NAD(P)^+$ by hydride donors

Rh nanoparticles dispersed in polyvinylpyrrolidone (Rh-PVP) were used for the visible-light-driven selective NADH production in the presence of a sacrificial electron donor, triethanolamine (TEOA), and a photosensitizer, zinc *meso*-5,10,15,20-tetrakis-(4-sulfonatophenyl)porphyrin (ZnTPPS), in the aqueous media, as shown in Scheme 13. It was confirmed that the reduction product of NAD^+ with ZnTPPS and Rh-PVP was only 1,4-NADH.[83] The photocatalytic reaction was started by electron transfer from ZnTPPS* to Rh-PVP by static quenching.[83] NAD^+ is adsorbed onto the surface of Rh-PVP by the carbonyl of the amide, similar to the Rh complex.[47,54] The hydride species at the surface of Rh-PVP attacks the C4 position of nicotinamide and forms 1,4-NADH directly (Scheme 14a).[83] Another possible mechanism is the interaction of NAD^+ with an absorbed H atom on the surface of Rh-PVP coupled with an electron transfer (Scheme 14b).[83] In any case, the hydride transfer is the key to avoid the radical intermediate and NAD dimer formation.[83]

When Rh-PVP was replaced by $[Cp^*Rh(bpy)(H_2O)]^{2+}$, photocatalytic reduction of NAD^+ by TEOA with ZnTPPS also occurred to produce 1,4-NADH selectively.[84,85] ZnTPPS can be replaced by various photoredox catalysts such as Ir complexes (Scheme 15),[86] Ru complexes,[63,87] inorganic semiconductors,[88] metal–organic frameworks (MOFs),[89] conjugated porous polymers

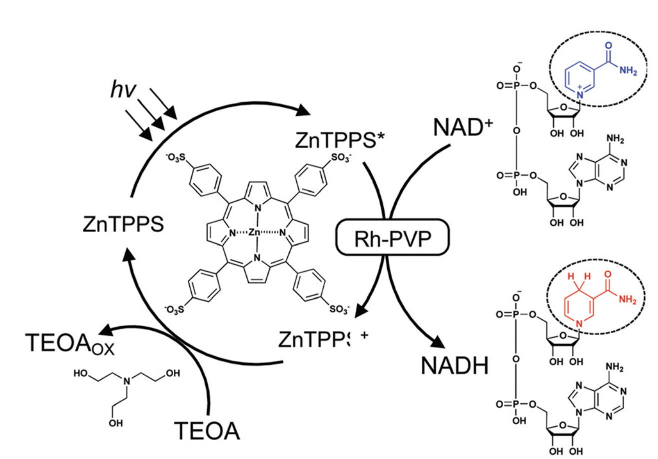

Scheme 13 Scheme of visible-light-driven NADH regeneration using the system composed of TEOA as an electron donor, ZnTPPS as a photosensitizer, Rh-PVP as a catalyst and NAD^+. Reprinted with permission from ref. 83. Copyright 2021, Royal Society of Chemistry.

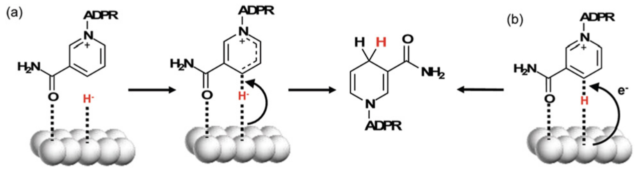

Scheme 14 Plausible mechanism of NADH regeneration using Rh-PVP by (a) H^- transfer or (b) adsorbed $H^\bullet$/electron transfer. Reprinted with permission from ref. 83. Copyright 2021, Royal Society of Chemistry.

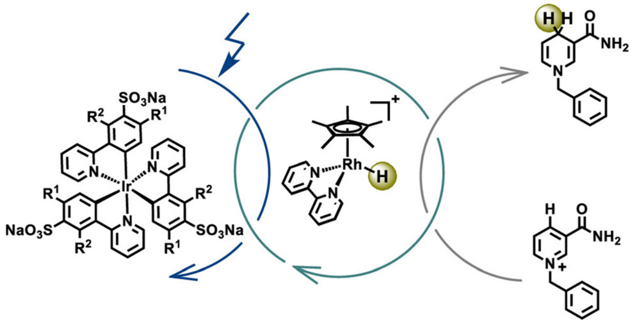

Scheme 15 Photochemical production of 1,4-BNAH using a rhodium catalyst ($[Cp^*Rh(bpy)(H_2O)]^{2+}$) with water soluble iridium(III) photosensitizers and TEOA for the regioselective BNA^+ reduction to 1,4-BNAH by TEOA. Reprinted with permission from ref. 86. Copyright 2023, American Chemical Society.

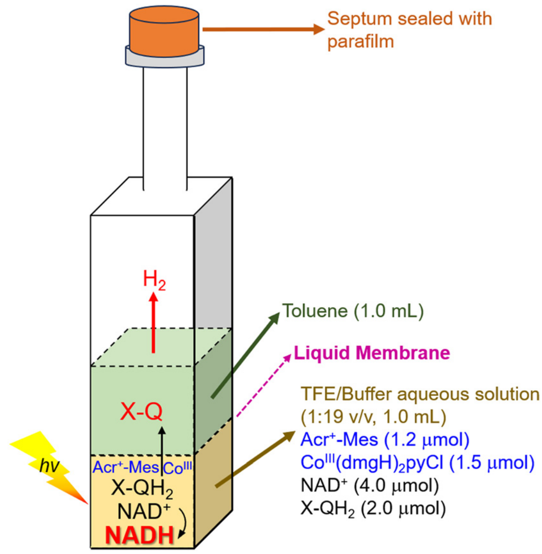

Fig. 6 A quartz cell employed for the PSI model reaction: photo-driven NAD^+ reduction by X-QH_2 in toluene (upper part) and a borate buffer/TFE mixed solution (v/v 19 : 1; lower part) containing X-QH_2 (2.0×10^{-6} mol), NAD^+ (4.0×10^{-6} mol), Acr^+-Mes (1.2×10^{-6} mol) and $Co^{III}(dmgH)_2pyCl$ (1.5×10^{-6} mol) to produce 1,4-NADH under photoirradiation of Acr^+-Mes in the aqueous/TFE phase. Reprinted with permission from ref. 100. Copyright 2024, American Chemical Society.

(CPPs)[90] and quantum dots (QDs)[91,92] for regioselective reduction of BNA^+ (or NAD^+) to 1,4-BNAH (or 1,4-NADH) with use of TEOA [or triethylamine (TEA)] as a hydride donor.

6. A PSI functional model

In photosynthesis, PQH_2 reduces $NADP^+$ regioselectively to generate 1,4-NADPH *via* charge separation in the photosynthetic reaction centre (PRC) in PSI [eqn (2)].[1] The first molecular model of PSI for NAD(P)H production has been reported by use of a hydroquinone derivative (X-QH_2) as a PQH_2 model compound, which regioselectively generates 1,4-NADH using a PRC model compound, 9-mesityl-10-methylacridinium ion (Acr^+-Mes),[93–96] and the NAD^+ reduction catalyst, $Co^{III}(dmgH)_2pyCl$,[97–99] under visible light irradiation [eqn (3)].[100]

$$PQH_2 + NAD(P)^+ \xrightarrow[PSI]{h\nu} PQ + NAD(P)H + H^+ \quad (2)$$

$$X\text{-}QH_2 + NAD^+ \xrightarrow[Acr^+\text{-Mes},\,Co^{III}(dmgH)_2pyCl]{h\nu} X\text{-}Q + NADH + H^+ \quad (3)$$

$$NADH + H^+ \xrightarrow[Acr^+\text{-Mes},\,Co^{III}(dmgH)_2pyCl]{h\nu} NAD^+ + H_2 \quad (4)$$

A quartz cell was used for the PSI model reaction [eqn (3)] in the two phases separated by a liquid membrane under visible light irradiation (Fig. 6).[100] NADH was produced by the photocatalytic reduction of NAD^+ by Cl_4QH_2 used as a PQH_2 model compound, being detected by HPLC measurements. On the other hand, evolution of H_2 was detected by GC (Fig. 7a).[100] NAD^+ is reduced regioselectively to 1,4-NADH, which is converted to H_2 at the later stage of the NADH production (Fig. 7a) as given by eqn (4).[100] The final yield for the conversion from NADH to H_2 was almost 20%.[100]

Cl_4QH_2 was converted to Cl_4Q [eqn (3)] as indicated by UV-vis absorption spectral changes in Fig. 7b.[100] When NAD^+ was replaced by an NAD^+ model compound (BNA^+), 1,4-BNAH was also selectively produced (Fig. 7c), accompanied by formation of Cl_4Q (Fig. 7d).[100] At prolonged irradiation time, O_2 is consumed by the photocatalytic oxidation of NADH or BNAH to produce H_2O_2. The photocatalytic mechanism of regioselective reduction of NAD^+ by QH_2 with a PRC model compound (Acr^+-Mes) and an NAD^+ reduction catalyst ($Co^{III}(dmgH)_2pyCl$) (Scheme 16) is virtually the same as the case of photocatalytic H_2 evolution from X-QH_2 with Acr^+-Mes and $Co^{III}(dmgH)_2pyCl$.[100] Firstly, photoexcitation of Acr^+-Mes in the aqueous/TFE phase results in intramolecular electron transfer from the Mes moiety to the singlet excited state of the Acr^+ moiety to produce the singlet electron-transfer (ET) state, followed by intersystem crossing to form the triplet ET state [$^3(Acr^\bullet$-$Mes^{\bullet+})$],[93–95] which undergoes the ET oxidation of X-QH_2 by the $Mes^{\bullet+}$ moiety to produce X-$QH_2^{\bullet+}$ as well as the ET reduction of $Co^{III}(dmgH)_2pyCl$ by the $Acr^\bullet$ moiety to produce $[Co^{II}(dmgH)_2pyCl]^-$.[100] X-$QH_2^{\bullet+}$ is deprotonated to produce the semiquinone radical (X-$QH^\bullet$),[100] followed by hydrogen atom transfer from X-$QH^\bullet$ to $[Co^{II}(dmgH)_2pyCl]^-$ to produce X-Q and the Co(III)-hydride complex ($[Co(H)(dmgH)_2pyCl]^-$).[100] Then, a H^- transfer from the Co(III)-hydride complex to NAD^+ proceeds *via* a six-membered ring transition state, where the hydride ion

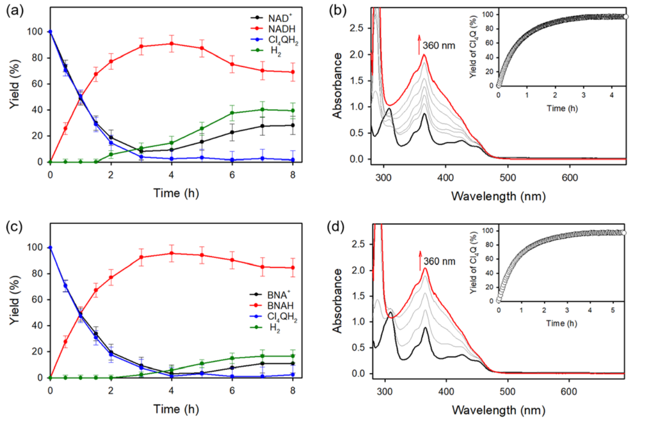

Fig. 7 (a) and (c) Time courses of a PSI model reaction: generation of (a) NADH and (c) BNAH in the photocatalytic reduction of (a) NAD^+ (4.0×10^{-6} mol) and (c) BNA^+ (4.0×10^{-6} mol), respectively, by Cl_4QH_2 (2.0×10^{-6} mol) with a PRC model compound (Acr^+-Mes: 1.5×10^{-6} mol) and $Co^{III}(dmgH)_2pyCl$ (NAD^+ reduction catalyst: 1.2×10^{-6} mol). (b) and (d) Visible absorption spectral changes in the photocatalytic reduction of (b) NAD^+ (4.0×10^{-6} mol) and (d) BNA^+ (4.0×10^{-6} mol) by Cl_4QH_2 (2.0×10^{-6} mol) with Acr^+-Mes (1.5×10^{-6} mol) and $Co^{III}(dmgH)_2pyCl$ (1.2×10^{-6} mol) in a toluene/TFE/borate buffer (v/v/v 40 : 1 : 19; 3.0 mL) at 298 K. Insets show time profiles of the formation of Cl_4Q. Reprinted with permission from ref. 100. Copyright 2024, American Chemical Society.

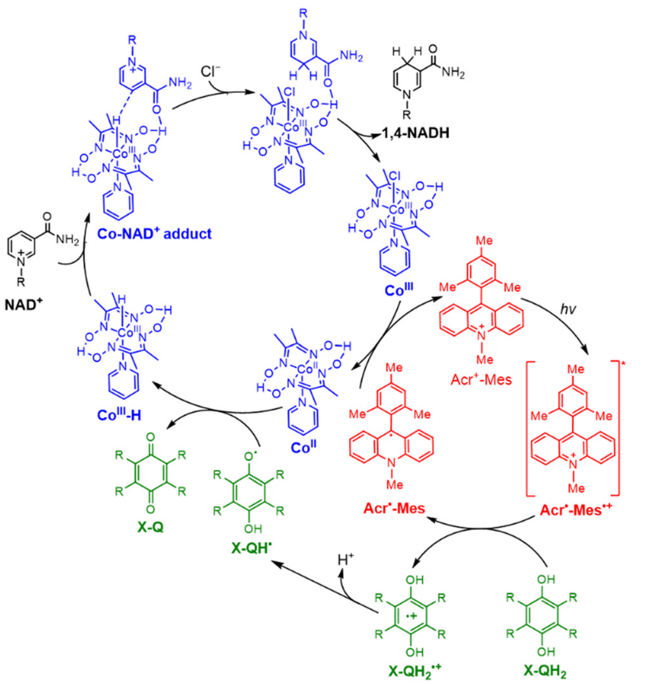

Scheme 16 Proposed mechanism of a PSI model reaction: the photocatalytic NAD^+ reduction to 1,4-NADH by X-QH_2 with a PRC model compound (Acr^+-Mes) and a NAD^+ reduction catalyst ($Co^{III}(dmgH)_2pyCl$). Reprinted with permission from ref. 100. Copyright 2024, American Chemical Society.

interacts with the C4-position of NAD^+ to yield 1,4-NADH regioselectively.[100] No other regioisomers, such as 1,2- and 1,6-NADH, were produced in the photocatalytic reduction of NAD^+ by X-QH_2 with Acr^+-Mes and $Co^{III}(dmgH)_2pyCl$ (Scheme 16).[100]

7. Photocatalytic reduction of $NAD(P)^+$ to NAD(P)H by water

The same photocatalytic system for the water splitting has been used to achieve the reduction of $NAD(P)^+$ to NAD(P)H by H_2O, accompanied by oxidation of H_2O to O_2 as shown in Fig. 8.[100,101] Photoirradiation of a mixed solution (two phase) of toluene, TFE and borate buffer (v/v/v 50 : 1 : 49; pH = 7.0) containing Cl_4Q and $[(N4Py)Fe^{II}]^{2+}$ in the left cell and a mixed solution (two phase) of toluene, TFE and borate buffer (v/v/v 50 : 1 : 49; pH = 7.0) containing $NAD(P)^+$ [or an NAD^+ model compound, 1-benzyl-3-carbamoylpyridinium cation (BNA^+)], Acr^+-Mes and $Co^{III}(dmgH)_2pyCl$ in the right cell resulted in regioselective formation of 1,4-NAD(P)H (or 1,4-BNAH) with almost 100% yield on the basis of the initial concentration of $NAD(P)^+$ (or BNA^+) used in the right cell together with production of O_2 in the left cell.[100] The TON for the production of NADH was 24, 16 and 12 on the basis of the initial concentrations of Cl_4Q, $Co^{III}(dmgH)_2pyCl$ and Acr^+-Mes, respectively.[100] Thus, Cl_4Q, $Co^{III}(dmgH)_2pyCl$ and Acr^+-Mes act as combined catalysts for the overall photocatalytic $NAD(P)^+$ reduction to 1,4-NAD(P)H by H_2O.[100] The photocatalytic $NAD(P)^+$ reduction occurred similarly when Cl_4QH_2 was replaced by hydroquinone (QH_2) and tetramethylhydroquinone (Me_4QH_2). Thus, a substituted *p*-benzoquinone (X-Q) generally acts as a plastoquinone (PQ) analogue, which is a redox catalyst in the photosynthesis

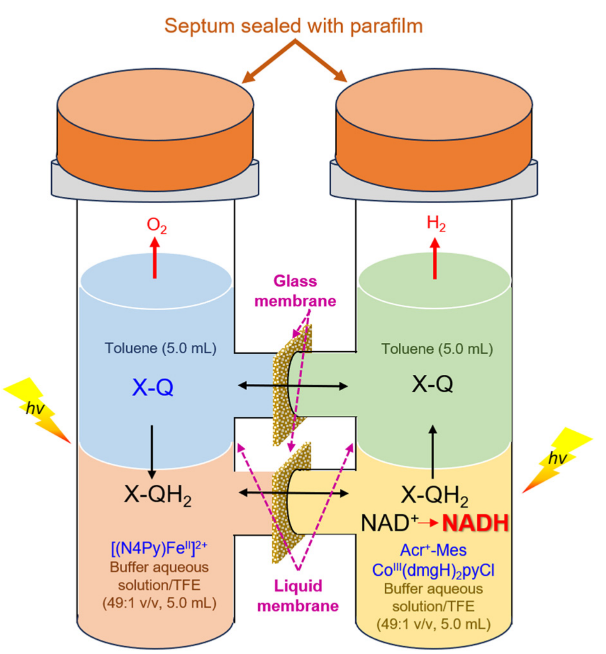

Fig. 8 A photochemical O-type quartz tube employed for molecular photosynthesis: photocatalytic regioselective NAD^+ reduction by H_2O to produce 1,4-NADH by combining PSI and PSII model systems. Reprinted with permission from ref. 100. Copyright 2024, American Chemical Society.

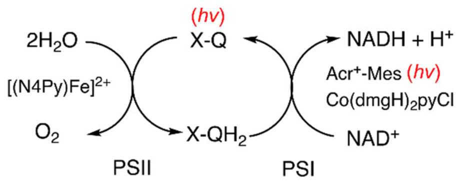

Scheme 17 Photocatalytic cycle for photocatalytic regioselective NAD^+ reduction by H_2O to produce 1,4-NADH and O_2, achieved by combining PSI and PSII molecular models. Reprinted with permission from ref. 100. Copyright 2024, American Chemical Society.

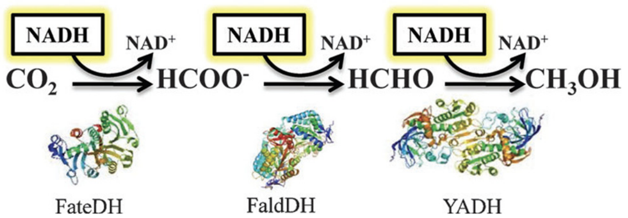

Scheme 18 Reduction scheme of CO_2 to methanol by three dehydrogenase enzymes (FateDH, FaldDH and YADH). Reprinted with permission from ref. 102. Copyright 2013, Royal Society of Chemistry.

(Scheme 17).[100] The ratio of production of O_2 : NADH was 1 : 2, agreeing with the stoichiometry of photosynthesis [eqn (1)].[100] Over long periods of light exposure, however, the concentration of O_2 gradually decreased and the production of NADH ceased because H_2 was produced by the reaction of NADH with H^+ [eqn (4)].[100]

Once NADH is obtained by photocatalytic regioselective reduction of NAD^+ by H_2O (Scheme 17), NADH can reduce CO_2 to methanol by using three dehydrogenases as shown in Scheme 18, where CO_2 is reduced to formate by the catalysis of formate dehydrogenase (FateDH), then formate is further reduced to formaldehyde by the catalysis of formaldehyde dehydrogenase (FaldDH) and finally methanol is obtained by the catalysis of alcohol dehydrogenase (YADH).[102] In the overall reaction, three equivalents of NADH are required to reduce CO_2 to methanol.[102] The optimized ratio of the three polyenzymes, *i.e.*, FateDH, FaldH and YADH, was found to be 0.010, 0.15 and 0.75 g L^{-1} of commercially available enzymatic powder, respectively.[102] Immobilization of the enzymes provides not only stabilisation and easier use, but also improved enzymatic activity.[103–105]

8. Conclusion and perspectives

Electrocatalytic reduction of $NAD(P)^+$ to 1,4-NAD(P)H has been achieved using Rh(III)–H complexes, which undergo hydride transfer to $NAD(P)^+$ with the interaction of the amide group of $NAD(P)^+$ with the metal centre to enable the regioselective reduction. The photoelectrocatalytic reduction of $NAD(P)^+$ to 1,4-NAD(P)H has lowered the applied potential required for the $NAD(P)^+$ reduction. The regioselective reduction of $NAD(P)^+$ has also been achieved by hydrogenation of $NAD(P)^+$ with H_2, catalysed by metal complexes. Photocatalytic reduction of $NAD(P)^+$ to 1,4-NADH can be made possible by combining photoredox catalysts and $NAD(P)^+$ reduction catalysts in the presence of a sacrificial electron and proton donor such as TEOA and TEA. When hydroquinone derivatives were employed as plastoquinol analogues in a photosystem I molecular model system, photocatalytic $NAD(P)^+$ reduction by hydroquinone derivatives occurred efficiently by using a simple photosynthetic reaction centre model, 9-mesityl-10-methylacridininum ion (Acr^+-Mes), and an $NAD(P)^+$ reduction catalyst, $Co^{III}(dmgH)_2pyCl$, under photoirradiation to produce only 1,4-NAD(P)H and *p*-benzoquinone derivatives (plastoquinone analogues). This photosystem I model has been combined with a photosystem II model in which water is oxidized by plastoquinone analogues to achieve the stoichiometry of photosynthesis, *i.e.*, photocatalytic reduction of $NAD(P)^+$ to 1,4-NAD(P)H by water used as a reductant. Once NAD(P)H is produced by regioselective reduction of $NAD(P)^+$ by H_2O using solar energy, reduction of various substrates, including CO_2 reduction, can occur through a combination of NAD(P)H dependent enzymes and PSI and PSII molecular models, providing a promising method for production of value-added products using water as a reductant and CO_2 as a carbon source. The activity and stability of photoredox catalysts and $NAD(P)^+$ reduction catalysts have yet to be improved for future practical applications.

Data availability

No primary research results, software or code have been included and no new data were generated or analysed as part of this review.

Conflicts of interest

There are no conflicts to declare.

Acknowledgements

The authors gratefully acknowledge the significant contributions of their collaborators and coworkers cited in the listed references and support from JSPS (23K04686 to S.F.) and NRF of Korea (NRF-2023R1A2C1007668 to Y.-M. L., NRF-2022H1D3A2A01045098 to S. F. and NRF-2021R1A3B1076539 to W. N.).

Notes and references

1 S. A. Watson and G. P. McStay, *Int. J. Mol. Sci.*, 2020, **21**, 7254.
2 S. Yoshikawa and A. Shimada, *Chem. Rev.*, 2015, **115**, 1936–1989.
3 A. Shimada, T. Tsukihara and S. Yoshikawa, *Front. Chem.*, 2023, **11**, 1108190.
4 M. Wikström, K. Krab and V. Sharma, *Chem. Rev.*, 2018, **118**, 2469–2490.
5 S. M. Adam, G. B. Wijeratne, P. J. Rogler, D. E. Diaz, D. A. Quist, J. J. Liu and K. D. Karlin, *Chem. Rev.*, 2018, **118**, 10840–11022.
6 S. Panda, H. Phan and K. D. Karlin, *J. Inorg. Biochem.*, 2023, **249**, 112367.

7 G. C. Schröder, M. S. Smit and D. J. Opperman, *Curr. Opin. Green Sustain. Chem.*, 2023, 39, 100734.
8 I. G. Denisov, T. M. Makris, S. G. Sligar and I. Schlichting, *Chem. Rev.*, 2005, **105**, 2253–2277.
9 L. Zhang and Q. Wang, *ChemBioChem*, 2022, **23**, e20210043.
10 J. He, X. Liu and C. Li, *Molecules*, 2024, **29**, 2480.
11 S. Shaik, S. Cohen, Y. Wang, H. Chen, D. Kumar and W. Thiel, *Chem. Rev.*, 2010, **110**, 949–1017.
12 F. P. Guengerich, *Chem. Res. Toxicol.*, 2008, **21**, 70–83.
13 D. Shevela, J. F. Kern, G. Govindjee and J. Messinger, *Photosynth. Res.*, 2023, **156**, 279–307.
14 N. Nelson and C. F. Yocum, *Annu. Rev. Plant Biol.*, 2006, **57**, 521–565.
15 M. M. Najafpour and S. I. Allakhverdiev, *J. Photochem. Photobiol., B*, 2015, **152**, 173–175.
16 A. Stirbet, D. Lazár, Y. Guo and G. Govindjee, *Ann. Bot.*, 2020, **126**, 511–537.
17 R. Siedentop and K. Rosenthal, *Int. J. Mol. Sci.*, 2022, **23**, 3605.
18 J. Britton, S. Majumdar and G. A. Weiss, *Chem. Soc. Rev.*, 2018, **47**, 5891–5918.
19 S. Mordhorst and J. N. Andexer, *Nat. Prod. Rep.*, 2020, **37**, 1316–1333.
20 R. A. Sheldon and D. Brady, *ACS Sustainable Chem. Eng.*, 2021, **9**, 8032–8052.
21 R. A. Sheldon and J. M. Woodley, *Chem. Rev.*, 2018, **118**, 801–838.
22 S. Huang, G. Chen and G. Ouyang, *Chem. Soc. Rev.*, 2022, **51**, 6824–6863.
23 K.-Y. Wang, J. Zhang, Y.-C. Hsu, H. Lin, Z. Han, J. Pang, Z. Yang, R.-R. Liang, W. Shi and H.-C. Zhou, *Chem. Rev.*, 2023, **123**, 5347–5420.
24 H. Wu, C. Tian, X. Song, C. Liu, D. Yang and Z. Jiang, *Green Chem.*, 2013, **15**, 1773–1789.
25 S. Fukuzumi, Y.-M. Lee and W. Nam, *J. Inorg. Biochem.*, 2019, **199**, 110777.
26 Y. S. Lee, R. Gerulskis and S. D. Minteer, *Curr. Opin. Biotechnol*, 2022, **73**, 14–21.
27 G. Zhao, C. Yang, W. Meng and X. Huang, *J. Mater. Chem. A*, 2024, **12**, 3209–3229.
28 V. K. Sharma, J. M. Hutchison and A. M. Allgeier, *ChemSusChem*, 2022, **15**, e202200888.
29 S. Immanuel, R. Sivasubramanian, R. Gul and M. A. Dar, *Chem. – Asian J.*, 2020, **15**, 4256–4270.
30 K. Bachosz, J. Zdarta, M. Bilal, A. S. Meyer and T. Jesionowski, *Sci. Total Environ.*, 2023, **868**, 161630.
31 S. Fukuzumi, Y.-M. Lee and W. Nam, *iScience*, 2024, **27**, 110694.
32 Y. H. Hong, Y.-M. Lee, W. Nam and S. Fukuzumi, *ACS Catal.*, 2023, **13**, 308–341.
33 Y. H. Hong, J. Jung, T. Nakagawa, N. Sharma, Y.-M. Lee, W. Nam and S. Fukuzumi, *J. Am. Chem. Soc.*, 2019, **141**, 6748–6754.
34 Y. Zhang and J. Liu, *Curr. Opin. Electrochem.*, 2024, **46**, 101506.
35 Y. Li, G. Liu, W. Kong, S. Zhang, Y. Bao, H. Zhao, L. Wang, L. Zhou and Y. Jiang, *Green Chem. Eng.*, 2024, **5**, 1–15.
36 A. Weckbecker, H. Grçger and W. Hummel, *Adv. Biochem. Eng. Biotechnol.*, 2010, **120**, 195–242.
37 S. Immanuel and R. Sivasubramanian, *Mater. Sci. Eng. B*, 2020, 114705.
38 F. Liu, C. Ding, S. Tian, S.-M. I. Lu, C. Feng, D. Tu, Y. Liu, W. Wang and C. Li, *Chem. Sci.*, 2022, **13**, 13361–13367.
39 H. Jaegfeldt, *Bioelectrochem. Bioenerg.*, 1981, **8**, 355–370.
40 I. Ali, A. Gill and S. Omanovic, *Chem. Eng. J.*, 2012, **188**, 173–180.
41 I. Ali and S. Omanovic, *Int. J. Electrochem. Sci.*, 2013, **8**, 4283–4304.
42 I. Ali, N. Ullah, M. A. McArthur, S. Coulombe and S. Omanovic, *Can. J. Chem. Eng.*, 2018, **96**, 68–73.
43 N. H. A. Besisa, K.-S. Yoon, T. G. Noguchi, H. Kobayashi and M. Yamauchi, *ACS Sustainable Chem. Eng.*, 2024, **12**, 9874–9881.
44 R. Wienkamp and E. Steckhan, *Angew. Chem., Int. Ed. Engl.*, 1982, **21**, 782–783.
45 R. Ruppert, S. Herrmann and E. Steckhan, *Tetrahedron Lett.*, 1987, **28**, 6583–6586.
46 E. Steckhan, S. Herrmann, R. Ruppert, E. Dietz, M. Frede and E. Spika, *Organometallics*, 1991, **10**, 1568–1577.
47 H. C. Lo, O. Buriez, J. B. Kerr and R. H. Fish, *Angew. Chem., Int. Ed.*, 1999, **38**, 1429–1432.
48 C. L. Pitman, O. N. L. Finster and A. J. M. Miller, *Chem. Commun.*, 2016, **52**, 9105–9108.
49 J. D. Blakemore, E. S. Hernandez, W. Sattler, B. M. Hunter, L. M. Henling, B. S. Brunschwig and H. B. Gray, *Polyhedron*, 2014, **84**, 14–18.
50 B. Tan, D. P. Hickey, R. D. Milton, F. Giroud and S. D. Minteer, *J. Electrochem. Soc.*, 2015, **162**, H102–H107.
51 W. Li, C. Zhang, Z. Zheng, X. Zhang, L. Zhang and A. Kuhn, *ACS Appl. Mater. Interfaces*, 2022, **14**, 46673–46681.
52 F. Liu, W. Shi, S. Tian, Y. Zhou, C. Feng, C. Ding and C. Li, *J. Phys. Chem. C*, 2024, **128**, 5927–5933.
53 S. Tian, G. Long, P. Zhou, F. Liu, X. Zhang, C. Ding and C. Li, *J. Am. Chem. Soc.*, 2024, **146**, 15730–15739.
54 A. Azem, F. Man and S. Omanovic, *J. Mol. Catal. A: Chem.*, 2004, **219**, 283–299.
55 I. Ali, T. Khan and S. Omanovic, *J. Mol. Catal. A: Chem.*, 2014, **387**, 86–91.
56 A. Damian, K. Maloo and S. Omanovic, *Chem. Biochem. Eng. Q.*, 2007, **21**, 21–32.
57 V. Ganesan, D. Sivanesan and S. Yoon, *Inorg. Chem.*, 2017, **56**, 1366–1374.
58 M. Chrzanowska, A. Katafias and R. van Eldik, *Inorg. Chem.*, 2020, **59**, 14944–14953.
59 R. Ruppert, S. Herrmann and E. Steckhan, *J. Chem. Soc., Chem. Commun.*, 1988, 1150–1151.
60 V. Ganesan, J. J. Kim, J. Shin, K. Park and S. Yoon, *Inorg. Chem.*, 2022, **61**, 5683–5690.
61 F. Chen, J. J. Soldevila-Barreda, I. Romero-Canelón, J. P. C. Coverdale, J.-I. Song, G. J. Clarkson, J. Kasparkova, A. Habtemariam, V. Brabec, J. A. Wolny, V. Schünemann and P. J. Sadler, *Dalton Trans.*, 2018, **47**, 7178–7189.
62 F. Chen, I. Romero-Canelón, J. J. Soldevila-Barreda, J.-I. Song, J. P. C. Coverdale, G. J. Clarkson, J. Kasparkova, A. Habtemariam, M. Wills, V. Brabec and P. J. Sadler, *Organometallics*, 2018, **37**, 1555–1566.
63 Y. Matsubara, K. Koga, A. Kobayashi, H. Konno, K. Sakamoto, T. Morimoto and O. Ishitani, *J. Am. Chem. Soc.*, 2010, **132**, 10547–10552.
64 M. Chrzanowska, A. Katafias, R. van Eldik and J. Conradie, *RSC Adv.*, 2022, **12**, 21191–21202.
65 M. Chrzanowska, A. Katafias and R. van Eldik, *Front. Chem.*, 2023, **11**, 1150164.
66 A. Bucci, S. Dunn, G. Bellachioma, G. M. Rodriguez, C. Zuccaccia, C. Nervi and A. Macchioni, *ACS Catal.*, 2017, **7**, 7788–7796.
67 L.-J. Zhao, C. Zhang, S. Zhang, X. Lv, J. Chen, X. Sun, H. Su, T. Murayama and C. Qi, *Inorg. Chem.*, 2023, **62**, 17577–17582.
68 L. Tensi, L. Rocchigiani, G. M. Rodriguez, E. Mosconi, C. Zuccaccia, F. De Angelis and A. Macchioni, *Catal. Sci. Technol.*, 2023, **13**, 6743–6750.
69 E. Lineberry, J. Kim, J. Kim, I. Roh, J.-A. Lin and P. Yang, *J. Am. Chem. Soc.*, 2023, **145**, 19508–19512.
70 E. J. Son, J. W. Ko, S. K. Kuk, H. Choe, S. Lee, J. H. Kim, D. H. Nam, G. M. Ryu, Y. H. Kim and C. B. Park, *Chem. Commun.*, 2016, **52**, 9723–9726.
71 S. H. Lee, G. M. Ryu, D. H. Nam, J. H. Kim and C. B. Park, *ChemSusChem*, 2014, **7**, 3007–3011.
72 B. Zhang, S. Xu, D. He, R. Chen, Y. He, W. Fa, G. Li and D. Wang, *J. Chem. Phys.*, 2020, **153**, 064703.
73 M. Chen, F. Liu, Y. Wu, Y. Li, C. Liu, Z. Zhao, P. Zhang, Y. Zhao, L. Sun and F. Li, *Chem. Commun.*, 2024, **60**, 3319–3322.
74 V. Massey, *Biochem. Soc. Trans.*, 2000, **28**, 283–296.
75 Y. Maenaka, T. Suenobu and S. Fukuzumi, *J. Am. Chem. Soc.*, 2012, **134**, 367–374.
76 Y. Maenaka, T. Suenobu and S. Fukuzumi, *Energy Environ. Sci.*, 2021, **5**, 7360–7367.
77 L. B. F. Browne, T. Sudmeier, M. A. Landis, C. S. Allen and K. A. Vincent, *Angew. Chem., Int. Ed.*, 2024, **63**, e202404024.
78 R. Mertens, L. Greiner, E. C. D. van den Ban, H. B. C. M. Haaker and A. Liese, *J. Mol. Catal. B*, 2003, **24–25**, 39–52.
79 H. A. Reeve, L. Lauterbach, O. Lenz and K. A. Vincent, *ChemCatChem*, 2015, **7**, 3480–3487.
80 M. Wang, Z. Zhao, C. Li, H. Li, J. Liu and Q. Yang, *Nat. Commun.*, 2022, **13**, 5699.
81 M. Wang, H. Dai and Q. Yang, *Angew. Chem., Int. Ed.*, 2023, **62**, e202309929.
82 D. Lovison, T. Berghausen, S. R. Thomas, J. Robson, M. Drees, C. Jandl, A. Pöthig, P. Mollik, D. P. Halter, W. Baratta and A. Casini, *ACS Catal.*, 2023, **13**, 10798–10823.
83 T. Katagiri and Y. Amao, *New J. Chem.*, 2021, **45**, 15748–15752.

84 M. Takeuchi and Y. Amao, *Chem. Lett.*, 2024, **53**, upae014.
85 M. Takeuchi and Y. Amao, *Bull. Chem. Soc. Jpn.*, 2023, **96**, 1206–1208.
86 M. R. Schreier, B. Pfund, D. M. Steffen and O. S. Wenger, *Inorg. Chem.*, 2023, **62**, 7636–7643.
87 Y. Matsubara and O. Ishitani, *Coord. Chem. Rev.*, 2023, **477**, 214955.
88 W. Lan, M. Wang, H. Dai and Q. Yang, *Front. Chem. Sci. Eng.*, 2024, **18**, 37.
89 Y. Chen, P. Li, J. Zhou, C. T. Buru, L. Đorđević, P. Li, X. Zhang, M. M. Cetin, J. F. Stoddart, S. I. Stupp, M. R. Wasielewski and O. K. Farha, *J. Am. Chem. Soc.*, 2020, **142**, 1768–1773.
90 Y. Wang, X. Yue, H. Zhao, L. Ma, L. Zhou, Y. Liu, X. Zheng, Y. He, G. Liu and Y. Jiang, *ChemSusChem*, 2024, e202301868.
91 C.-H. Gao, S.-M. Zhang, F.-F. Feng, S.-S. Hu, Q.-F. Zhao and Y.-Z. Chen, *J. Colloid Interface Sci.*, 2023, **652**, 1043–1052.
92 I. N. Chakraborty, V. Jain, P. Roy, P. Kumar, C. P. Vinod and P. P. Pillai, *ACS Catal.*, 2024, **14**, 6740–6748.
93 S. Fukuzumi, H. Kotani, K. Ohkubo, S. Ogo, N. V. Tkachenko and H. Lemmetyinen, *J. Am. Chem. Soc.*, 2004, **126**, 1600–1601.
94 T. Tsudaka, H. Kotani, K. Ohkubo, T. Nakagawa, N. V. Tkachenko, H. Lemmetyinen and S. Fukuzumi, *Chem. – Eur. J.*, 2017, **23**, 1306–1317.
95 S. Fukuzumi, K. Ohkubo and T. Suenobu, *Acc. Chem. Res.*, 2014, **47**, 1455–1464.
96 K. Ohkubo, S. Matsumoto, H. Asahara and S. Fukuzumi, *ACS Catal.*, 2024, **14**, 2671–2684.
97 J. L. Dempsey, B. S. Brunschwig, J. R. Winkler and H. B. Gray, *Acc. Chem. Res.*, 2009, **42**, 1995–2004.
98 J. A. Kim, S. Kim, J. Lee, J.-O. Baeg and J. Kim, *Inorg. Chem.*, 2012, **51**, 8057–8063.
99 Y. H. Hong, Y.-M. Lee, W. Nam and S. Fukuzumi, *Inorg. Chem.*, 2020, **59**, 14838–14846.
100 Y. H. Hong, M. Nilajakar, Y.-M. Lee, W. Nam and S. Fukuzumi, *J. Am. Chem. Soc.*, 2024, **146**, 5152–5161.
101 Y. H. Hong, Y.-M. Lee, W. Nam and S. Fukuzumi, *J. Am. Chem. Soc.*, 2022, **144**, 695–700.
102 R. Cazelles, J. Drone, F. Fajula, O. Ersen, S. Moldovan and A. Galarneau, *New J. Chem.*, 2013, **37**, 3721–3730.
103 C. Di Spiridione, M. Aresta and A. Dibenedetto, *Adv. Energy Sustainability Res.*, 2024, **5**, 2400081.
104 M. E. Aguirre, C. L. Ramírez and Y. Di Iorio, *Chem. – Eur. J.*, 2023, **29**, e202301113.
105 Y. Shu, W. Liang and J. Huang, *Green Chem.*, 2023, **25**, 4196–4221.

